journal of the mechanical behavior of biomedical materials 122 (2021) 104697

Contents lists available at ScienceDirect

Journal of the Mechanical Behavior of Biomedical Materials

journal homepage: www.elsevier.com/locate/jmbbm

Research paper

Mechanical alterations of the hippocampus in the APP/PS1 Alzheimer's disease mouse model

Nelda Antonovaite [a,*], Lianne A. Hulshof [b], Christiaan F.M. Huffels [b], Elly M. Hol [b], Wytse J. Wadman [c], Davide Iannuzzi [a]

[a] Department of Physics and Astronomy and LaserLaB, VU Amsterdam, The Netherlands
[b] Department of Translational Neuroscience, University Medical Center Utrecht, Brain Center, Utrecht University, Utrecht, The Netherlands
[c] Center for Neuroscience, Swammerdam Institute for Life Sciences, University of Amsterdam, The Netherlands

ARTICLE INFO

Keywords:
Brain mechanics
Alzheimer's disease
Viscoelasticity
Biomechanical testing

ABSTRACT

There is increasing evidence of altered tissue mechanics in neurodegeneration. However, due to difficulties in mechanical testing procedures and the complexity of the brain, there is still little consensus on the role of mechanics in the onset and progression of neurodegenerative diseases. In the case of Alzheimer's disease (AD), magnetic resonance elastography (MRE) studies have indicated viscoelastic differences in the brain tissue of AD patients and healthy controls. However, there is a lack of viscoelastic data from contact mechanical testing at higher spatial resolution. Therefore, we report viscoelastic maps of the hippocampus obtained by a dynamic indentation on brain slices from the APP/PS1 mouse model where individual brain regions are resolved. A comparison of viscoelastic parameters shows that regions in the hippocampus of the APP/PS1 mice are significantly stiffer than wild-type (WT) mice and have increased viscous dissipation. Furthermore, indentation mapping at the cellular scale directly on the plaques and their surroundings did not show local alterations in stiffness although overall mechanical heterogeneity of the tissue was high (SD~40%).

1. Introduction

Neurodegenerative diseases are difficult to research due to the complex biochemical processes and limited physical access to the brain. Neurodegenerative diseases are characterized by the accumulation of aberrant proteins, reactive gliosis and neural cell death. The exact molecular mechanism leading to the disease is often not known. In addition, in the past two decennia, several studies have indicated the relation between mechanical factors and brain functioning. For example, the mechanical sensitivity of neuronal and glial cells to the stiffness of environment has been demonstrated in cell culture experiments and *in vivo* by altered morphology, growth and other biochemical properties (Franze and Guck, 2010; Lacour et al., 2016; Moshayedi et al., 2014; Tomba et al., 2019; Franze, 2013; Koser et al., 2016; Georges et al., 2006). Moreover, in some neurodegenerative diseases, such as demyelinating disorders, the mechanical properties have been shown to change together with the structure, thereby raising questions about the involvement of mechanobiological processes in disease progression (Eberle et al., 2018; Streitberger et al., 2012; Urbanski et al., 2019).

Alzheimer's disease is a neurodegenerative disease and the most common form of dementia in the elderly. The exact molecular and cellular cause of dementia is still elusive, and effective drugs to halt or reverse the disease are still lacking. The pathology consists of the formation of extracellular plaques by the accumulation of amyloid β peptide (Aβ) and hyper-phosphorylated tau protein as intracellular neurofibrillary tangles (NFTs). Activated microglia and reactive astrocytes have been identified as the key players orchestrating chronic inflammatory response, linked to the severity of neuronal dysfunction in AD and are found accumulated around plaques similarly to glial scarring (Osborn et al., 2016; Fakhoury, 2018). Chronic neuroinflammation causes disease-related symptoms, such as loss of neurons and synapses ultimately leading to memory problems and dementia (Sasaguri et al., 2017). In addition to the underlying biological processes in AD, the investigation of mechanical properties received attention in recent years as a potential biomarker for early diagnosis, as shown by magnetic resonance elastography (MRE) studies where brain elasticity and viscosity decreased in AD human patients (Murphy et al., 2016; Hiscox et al., 2020; Levy Nogueira et al., 2016; Murphy et al., 2011; Gerischer et al., 2018; Kihan Park et al., 2019), and as a novel drug target for tissue regeneration (Hall et al., 2020; Mahumane et al., 2018).

AD is often studied on mouse models carrying human transgenes with AD-linked mutations in amyloid precursor protein (APP) and

* Corresponding author.
E-mail address: nelda.antonovaite@gmail.com (N. Antonovaite).

https://doi.org/10.1016/j.jmbbm.2021.104697
Received 29 December 2020; Received in revised form 26 June 2021; Accepted 3 July 2021
Available online 10 July 2021

Presenilin-1 (PSEN1) (Trinchese et al., 2004; Yan et al., 2009; Kamphuis et al., 2012; Galea et al., 2015). These mice exhibit extensive Aβ pathology and reactive gliosis in the hippocampus and cortex without tauopathy, which is suitable to study age-related synaptic and cognitive deficits during amyloid deposition (Trinchese et al., 2004; Sasaguri et al., 2017; Smit et al., 2021). In APPswe/PS1dE9 mouse model used in this study, amyloid plaques appear at 4 months of age (Garcia-Alloza et al., 2006; Ruan et al., 2009), contextual fear memory is impaired as early as 3 months (Vé et al., 2014; D'Amelio et al., 2011), spatial reference memory is affected at 6 months of age (Vé et al., 2014; Montarolo et al., 2013) and astrogliosis is detected at 6 months of age (Ruan et al., 2009; van Tijn et al., 2012; Vé et al., 2014)(see review (Smit et al., 2021)). Although experiments on mouse brain tissue allow using contact mechanical testing methods, which is considered being a gold standard, only two studies have reported Young's modulus values of cortex (Menal et al., 2018) and hippocampus (Zhao et al., 2019). Therefore, a more appropriate viscoelastic characterization of the hippocampus where amyloid plaques are present is needed. Although MRE can be used on humans as it noninvasively induces shear waves (<1 μm amplitude) from which one can calculate viscoelastic properties, the technique is limited to relatively high frequencies (10–100 Hz for humans Hiscox et al., 2016 and 200–1800 Hz for rodents Bigot et al., 2018) and a low spatial resolution (~mm), thus, contact mechanical testing is needed to provide reliable mechanical data at higher resolution and lower-frequency spectrum to shed some light on the mechanobiology of AD.

In this study, we hypothesized that mechanical properties of APP/PS1 mouse brain hippocampus are altered in comparison to WT. To test it, we performed oscillatory indentation mapping of hippocampal subregions of APP/PS1 and wild type (WT) mice brain tissue slices where results of the latter have been already reported (Antonovaite et al., 2018). Comparison between APP/PS1 and WT mice hippocampal subregions is presented in terms of the storage modulus and damping factor. To assess structural differences between APP/PS1 and WT mice hippocampus, a qualitative comparison of (immuno)histochemical stained images of brain components is made. Moreover, direct indentation mapping of the plaques and the surrounding tissue was carried out at a single-cell scale to assess the mechanical contribution of individual plaques.

2. Methods

2.1. Sample preparation for indentation measurements

4 animals of 6 and 9 month-old (2 and 2 mice, respectively) C57BL6/Harlan wild type (WT) mice, and 6 animals of 6 and 9 month-old (5 and 1 mice, respectively) APPswe/PS1dE9 (APP/PS1) double-transgenic mice, which were littermates to WT mice, were used for indentation experiments reported in Section 3.1 (Kamphuis et al., 2012). All experiments were performed by following protocols and guidelines approved by the Institutional Animal Care and Use Committee (UvA-DEC) operating under standards set by EU Directive 2010/63/EU. 2 animals of 9-month-old APPswe/PS1dE9 double-transgenic mice were used for indentation experiments reported in Section 3.2. Animal handling and experimental procedures were previously approved by the Animal Use Ethics Committee of the Central Authority for Scientific Experiments on Animals of the Netherlands (CCD, approval protocol AVD1150020174314). Experiments were performed according to the Directive of the European Parliament and of the Council of the European Union of 22 September 2010 (2010/63/EU).

The mice were decapitated, brains were dissected, and stored in an ice-cold carbonated 30% sucrose solution. Slices were cut in a horizontal plane with a thickness of approximately 300 μm using a VT1200S vibratome (Leica Biosystems, Germany) and placed to rest in artificial cerebrospinal fluid (aCSF) for 15 min in 32 °C and 1 h at room temperature. Afterward, a single brain slice was placed in a perfusion chamber coated with 0.05% poly(ethyleneimine) solution, stabilized with a harp, and supplied with aCSF solution at 1 ml/min flow rate. Slices from 3 to 4 mm of dorsal–ventral positions were used in the experiment to minimize the effects of structural variation along with the hippocampus. Indentation measurements were performed within 8 h after extraction at room temperature. Results from WT mice brain slices were published previously (see Antonovaite et al., 2018).

2.2. Dynamic indentation setup and measurement protocol on 300 μm thickness brain slices

The setup and measurement protocol used in this experiment has been described previously (Antonovaite et al., 2018). In short, the custom indenter was mounted on top of an inverted microscope (Nikon TMD-Diaphot, Nikon Corporation, Japan) to image the slice during the measurements with a 2 × magnification objective (Nikon Plan 2X, Nikon Corporation, Japan) and a CCD camera (WAT-202B, Watec), while a cantilever-based ferrule-top force sensor equipped with spherical tip was indenting the brain slice from the top. Fig. 1B shows a schematic drawing of the setup and a microscope image where the cantilever can be seen through the brain slice. The force sensors used for the experiments had cantilevers with the spring constant of 0.2–0.5 N/m and 60–105 μm bead radius. Indentation mapping was performed in indentation-depth controlled mode with the step size of 50–80 μm. Oscillations at 5.62 Hz frequency and 0.2 μm amplitude were superimposed on top of the loading ramp at an approximate strain rate of 0.01 s^{-1} (Fig. 1A) to reach 8.5–15 μm indentation-depth (depending on the sphere radius), which corresponds to 7.5% strain ($\epsilon = 0.2\sqrt{Rh/R}$) and fulfills small strain approximation $\epsilon < 8\%$ (Lin et al., 2009). Depth-dependent viscoelastic properties in terms of storage E' and loss E'' moduli, and damping factor tanδ were calculated using dynamic mechanical analysis (DMA) which assumes linear viscoelastic mechanical behavior (Herbert et al., 2008):

$$E'(\omega, h) = \frac{F_0}{h_0}\cos\delta\frac{\sqrt{\pi}}{2}\frac{(1-\nu^2)}{\sqrt{A}}, \quad (1)$$

$$E''(\omega, h) = \frac{F_0}{h_0}\sin\delta\frac{\sqrt{\pi}}{2}\frac{(1-\nu^2)}{\sqrt{A}} \quad (2)$$

$$\tan\delta(\omega, h) = \frac{E''(\omega)}{E'(\omega)} \quad (3)$$

where ω is the oscillation frequency, F_0 and h_0 are the amplitudes of oscillatory load and indentation-depth, respectively, δ is the phase-shift between indentation and load oscillations, $A = \pi a^2$ is the contact area, $a = \sqrt{hR}$ is the contact radius, ν is the Poisson's ratio of compressibility (we assume that brain is incompressible $\nu = 0.5$), h is the indentation-depth.

Measurements were carried out on 6 slices from 6 APP/PS1 mice of which one was 9-month-old and the others were 6-month-old, with 63–535 measurement points per slice and 1235 total number of indentations. During the same experiment, indentation measurements (n = 1029) were also performed on 5 slices from 4 WT mice (three 6-month-old and two 9-month-old) (Antonovaite et al., 2018). After the measurements, slices were stained with Methoxy X-04 (10 μM solution for 12 min), fixed in 4% paraformaldehyde (PFA) overnight at 4 °C, and imaged with a fluorescence microscope (Leica Microsystems, Wetzlar, Germany). Afterward, slices were stained with Hoechst nuclear stain and imaged again. The coordinates of the probe tip were converted into coordinates of the camera image by taking three images of the probe tip at three corners of the field of view. Then, coordinates of the indentation map were converted into image coordinates and drawn on the image of the brain slice. Next, the fluorescent image of the fixed brain slice was overlaid with the brightfield image of the live brain slice. Using the contrast in intensity from the brightfield image together with differences in cell density from nuclear staining, anatomical regions could be identified. Finally, each measured location was assigned to the corresponding region.

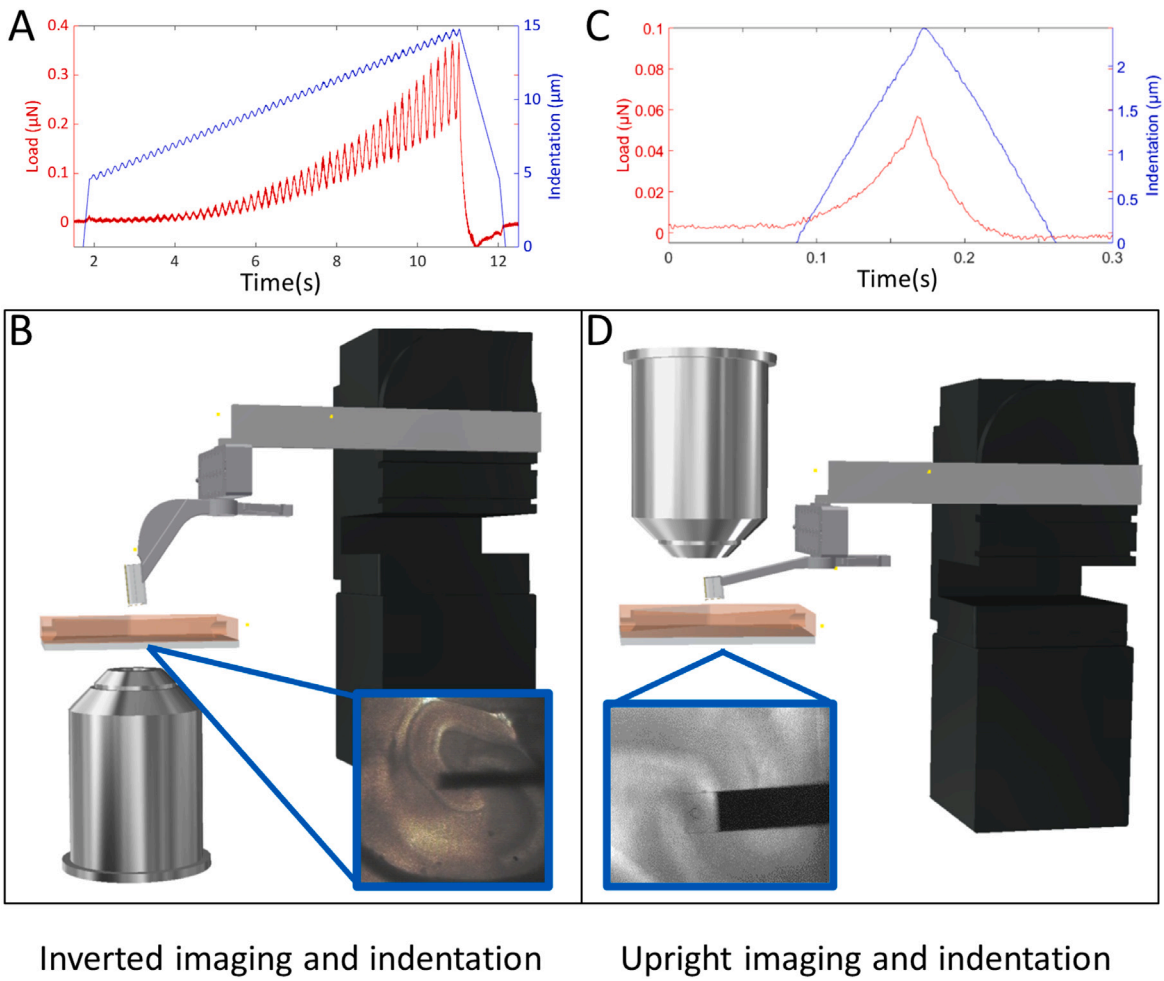

Fig. 1. Indentation setup and profiles. The oscillatory-ramp indentation profile (A) was used for viscoelastic characterization of the whole hippocampus at a tissue scale by using an inverted bright-field microscope and indenter (B) to localize the sphere of the probe (R = 60–105 μm) on top of the brain tissue. Static indentation profile (C) was used to measure elastic properties at a cell scale with an upright fluorescence microscope and indenter (D) by localizing the tip of the probe (R = 21 μm) above the stained plaque.

The second set of measurements was done with upright fluorescence microscope Axioskop 2 FS plus (Fig. 1D), where the probe was modified to have a transparent cantilever tip, half-size ferrule, and shallow angle holder to fit the probe under the long working distance objective (Plan-Neofluar x5/0.16, Zeiss). An indentation probe with spring constant of 0.23 N/m and tip size of 21 μm was used to make static indentation mapping (see Fig. 1C) with 5–9 μm step size at 30 μm/s piezo-transducer speed by indenting up to 3 μm indentation-depth (7.5% strain), which fulfills small strain approximation (Lin et al., 2009). The Young's modulus was obtained by fitting Hertz model (Ueber die, 2009). APP/PS1 slices were live stained with Methoxy X-04 (10 μM solution for 12 min) before the measurements to locate Aβ plaques by fluorescence microscopy (filter set DAPI-50LP-A-000, Semrock). 4 slices from 2 animals (one 6-month-old and one 9-month-old) were used in these experiments to obtain 6 indentation maps (n = 100–121 locations per map).

2.3. *(Immuno)histochemistry of 30* μm *thickness brain slices*

(Immuno)histochemistry (Section 3.3) was performed on three 6 months old WT and three APP/PS1 female littermate mice from Jackson Laboratories (Kamphuis et al., 2012). Animal handling and experimental procedures were previously approved by the Animal Use Ethics Committee of the Central Authority for Scientific Experiments on Animals of the Netherlands (CCD, approval protocol AVD1150020174314). Experiments were performed according to the Directive of the European Parliament and of the Council of the European Union of 22 September 2010 (2010/63/EU). Mice were anesthetized with 0.1 ml Euthanimal 20% (Alfasan 10020 UDD) and transcardially perfused with 1X PBS. Brains were removed and collected in 4% paraformaldehyde for 48 h before being transferred to 30% sucrose with sodium azide and stored at 4 °C. Before cutting, brains were frozen in isopentane and mounted using Tissue-Tek (Sakura). Using a cryostat, brains were sliced horizontally in 30 μm thick slices and collected in 1X PBS, which was then replaced by a cryopreservation medium (19% glucose, 37.5% ethylene glycol in 0.2 M PB with sodium azide) and stored at −20 °C until further processing.

Slices were washed 3 times with PBS before they were blocked with 10% Normal Donkey Serum (NDS, Jackson ImmunoResearch, 017-000-121) and 0.4% Triton-X in 1X PBS for one hour at RT. Sections were incubated with different primary antibodies (Rat-anti-MBP, Sigma-Aldrich MAB386, 1:1000, monoclonal; Rabbit-anti-GFAP, CiteAb Z0334, 1:1000, polyclonal; Mouse-anti-6E10 Amyloid-β, BioLegend SIG-39300, 1:1000, monoclonal) diluted in 200 μl 10% NDS and 0.4% Triton-X blocking medium ON at 4 °C. Thereafter, they were washed 3 times with 1X PBS and then incubated with 1:1000 secondary antibodies (Donkey-anti-Rat Cy3, Jackson ImmunoResearch 712-165-153; Donkey-anti-Mouse Alexa Fluor 488, Jackson ImmunoResearch 715-546-150; Donkey-anti-Mouse Alexa Fluor 594, Jackson ImmunoResearch 715-585-150; Donkey-anti-Rabbit Alexa Fluor 488, Jackson ImmunoResearch 711-545-152; Donkey-anti-Rabbit Alexa Fluor 594, Jackson ImmunoResearch 711-496-152) or 1:500 Wisteria floribunda

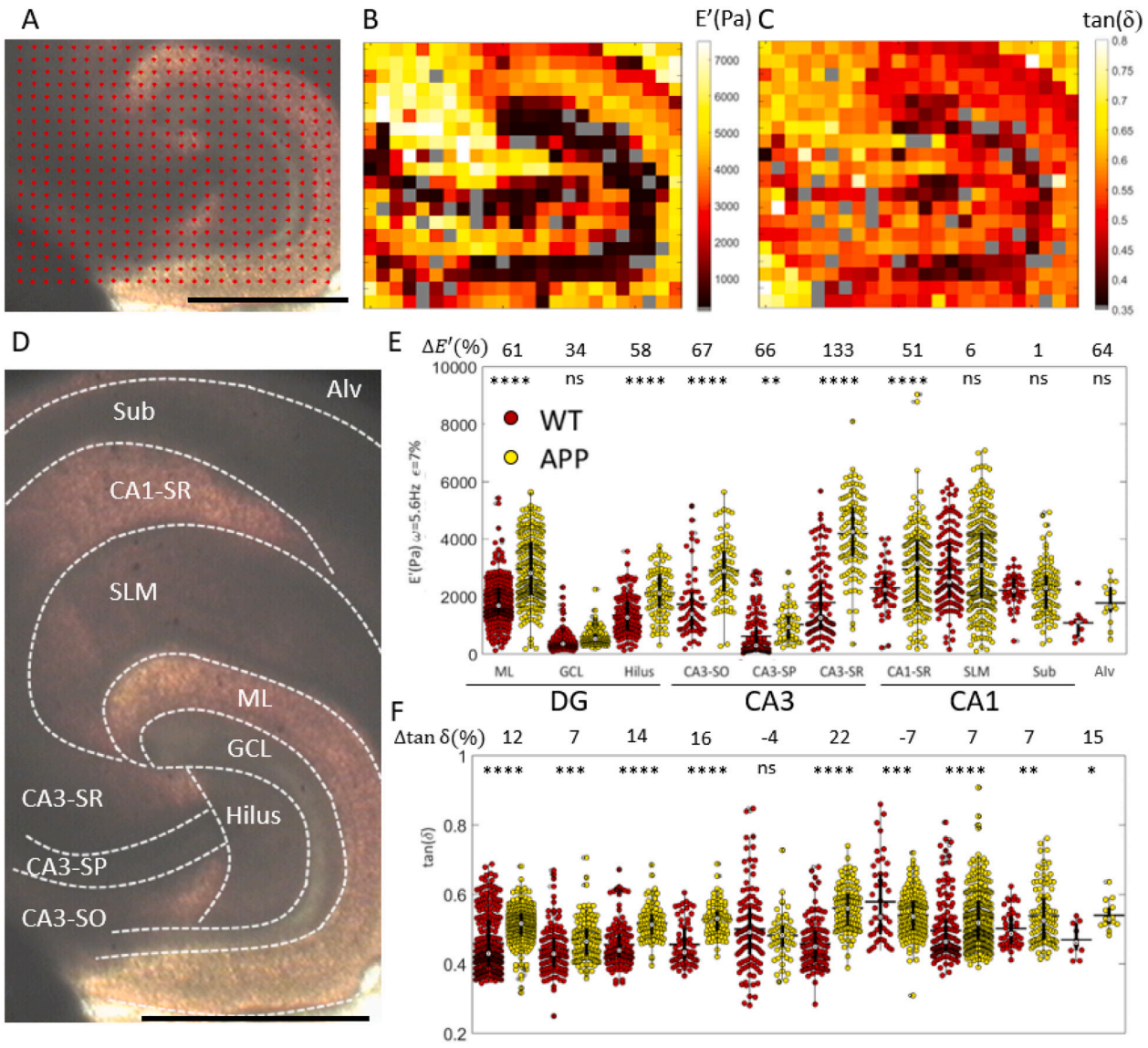

Fig. 2. (A) Red dots indicate indentation locations on a microscope image of the APP/PS1 mouse brain slice. (B) Corresponding color map of storage modulus E' and (C) damping factor tanδ obtained at 5.6 Hz oscillation frequency and 7% strain. (D) Hippocampal subregions were identified on the camera image of the slices with boundaries marked in dashed white lines. (E) Storage modulus E' and (F) damping factor tanδ values of WT (red) and APP (yellow) mice hippocampal subregions at 7±0.5% strain. Data is merged over multiple slices (2 to 6 depending on the region, see Table S.1). The white dot indicates the median value with the vertical black bar for 25th and 75th percentiles and horizontal bar for the mean value. Bonferroni corrected p-values for pairwise comparison of simple main effects are indicated with asterisks: ****p < 0.00001, ***p < 0.001,**p < 0.01, *p < 0.05, ns — non significant. Relative differences Δ(%) in estimated marginal means of storage modulus and damping factor are given above the graphs. Abbreviations: Alv — alveus, Sub — subiculum, SLM — stratum lacunosum moleculare, SR — stratum radiatum, SP — stratum pyramidale, SO — stratum oriens, ML — molecular layer, GCL — granule cell layer, dentate gyrus (DG) and cornus ammonis (CA1 and CA3). WT data has been reported previously (Antonovaite et al., 2018).

agglutinin (WFA) dye diluted in 200 μl 3.3% NDS and 0.13% Triton-X in 1X PBS ON at 4 °C, washed 3 times with 1x PBS and stained with 1:1000 Hoechst dissolved in 500 μl 1x PBS for 10 min at RT. Slices were washed 2 times with 1X PBS and 1 time with MilliQ before mounting them on microscope slides using Mowiol (10% Mowiol (Millipore, 475904), 0.1% diazabicyclo(2,2,2)-octane, 0.1 M Tris and 25% glycerol in H_2O; pH 8.5). Imaging was done with the Zeiss Axioscope.A1 epi-microscope operated with AxioVision software, using a 10x Plan-NeoFluar objective.

2.4. Statistics

Factorial (univariate) ANOVA analysis was used for statistical analysis with either storage modulus or damping factor as an independent variable and region, type of mice (WT or APP/PS1) or age as fixed factors. Data from different animals was merged as not all the same regions were tested in each animal, the number of indentation points varied between the animals and there was not enough evidence for age being a significant factor (region: $F(3,635) = 202.50$, $p<0.0005$; age: $F(1,636) = 0.31$; $p = 0.58$; interaction term: $F(3,635) = 14.69$, $p<0.0005$, when tested storage modulus data of ML, GCL, SLM and Hilus regions of 6- (n = 3) and 9-months-old (n = 2) WT animal slices). The test was followed by *post hoc* tests with Bonferroni correction for multiple comparisons was applied during statistical analysis of data using IBM SPSS Statistics software.

3. Results

3.1. Viscoelastic properties of APP/PS1 mouse brain hippocampus is altered in comparison to WT

The depth-controlled oscillatory indentation mapping was performed at 50–80 μm axial resolution to capture regional mechanical

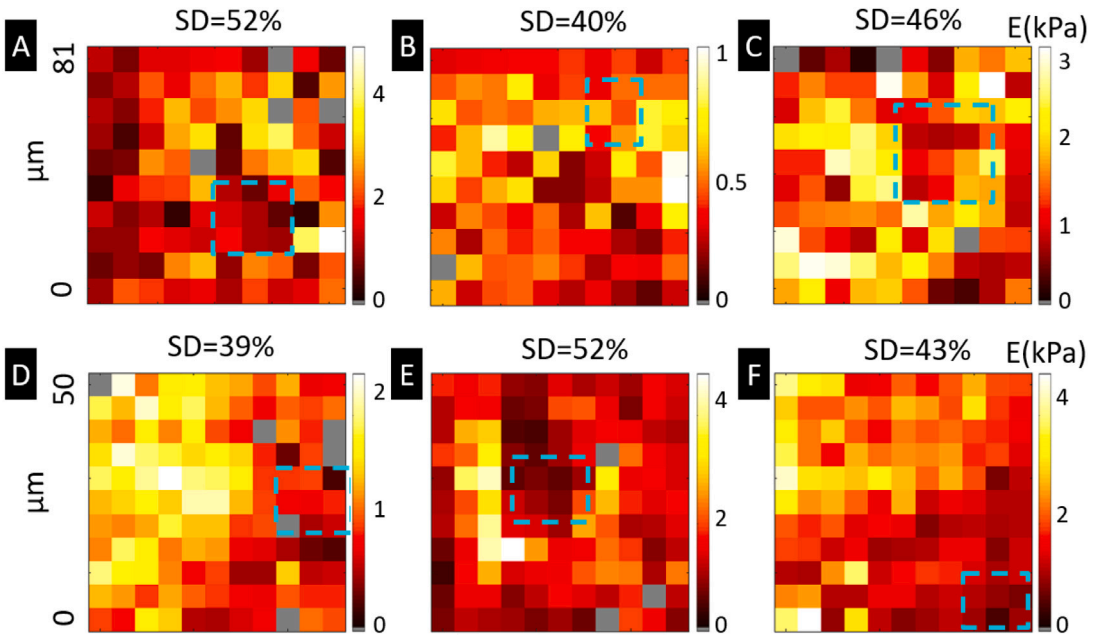

Fig. 3. (A–F) Maps of Young's modulus of APP/PS1 mice hippocampal regions with plaques obtained by fitting Hertz model up to 3 μm. The blue dashed line indicates the location of the plaque obtained from staining with Methoxy-X04. (A–C) Indentation mapping was performed on different slices from the same 6-month-old animal, regions (A) ML, (B) SLM/CA3-SR, (C) SLM at 9 μm step size. (D–F) Maps were obtained on one slice from a 9-month-old animal, regions (D) SLM, (E) CA3-SO, (F) Sub at 5 μm step size.

differences hippocampus. The indentation lines were selected to cross the dentate gyrus (DG) and Cornu Ammonis 1 (CA1) or the CA3 fields of the hippocampus. As an example, Fig. 2 A shows indentation locations on the camera image of the APP/PS1 mice brain slice of DG and CA3 regions and storage modulus E' and damping factor tanδ maps plotted at 7% strain (Fig. 2 B and C, respectively). Different anatomical regions can be identified in the storage modulus map because of the high mechanical heterogeneity of different brain regions, which are related to varying morphology of brain regions (also observed on WT brain slices where data has been already published in Antonovaite et al., 2018, 2020); differences in damping factor tanδ are less pronounced but still visible.

Each indentation location was assigned to one of 10 measured hippocampal subregions (see Fig. 2 D, Methods 2.2) and storage modulus E' and damping factor tanδ values at 7% strain are plotted in Fig. 2 E, F. 6- and 9-month-old data were merged considering that both age groups are adults and no obvious differences in viscoelastic parameters were found (see Section 2.4). The region, group of animals (WT or APP/PS1) and their interaction terms were significant factors for storage modulus ($F(9,2258) = 135.87$, $F(1,2258) = 298.26$, $F(9,2258) = 23.78$, respectively, $p < 0.0005$, factorial ANOVA) and damping factor ($F(9,2254) = 20.53$, $F(1,2254) = 186.09$, respectively, $F(9,2254) = 13.48$, $p < 0.0005$, factorial ANOVA). The storage modulus of APP/PS1 mouse hippocampus was 1.5 times higher when considering all regions together with estimated marginal means of 1.63 ± 0.05 kPa for WT and 2.39 ± 0.04 kPa for APP/PS1 hippocampus. At an individual region level, the simple main effect analysis showed that differences in storage modulus were significant for the majority of the regions with the relative increase $\Delta E'$ in these regions between 51 and 133% (Fig. 2 E). Moreover, the damping factor tanδ was 1.1 times higher for APP/PS1 than WT (0.522 ± 0.003 and 0.481 ± 0.003, respectively) when considering all regions together. At an individual region level, the damping factor was significantly higher for most of the regions with the relative increase Δtanδ between 7 and 22%, except for CA3-SP, where the difference was not significant, and CA1-SR, where it was significantly lower (see Fig. 2 F). An increase in storage modulus E' of APP/PS1 mouse hippocampus means that the material can resist more deformation while an increase in tanδ indicates that the loss modulus increased more than the storage modulus and, thus, the damping capability of the tissue, i.e. its fluid-like behavior, is larger.

In terms of mechanical heterogeneity, an elastic component (storage modulus) of mechanical behavior varies significantly between different regions, from 0.4 to 2.9 kPa for WT and from 0.6 to 4.2 kPa for APP/PS1 (estimated marginal means). Although damping is also different in different regions, it varies less, ranging between 0.44 and 0.58 for WT and between 0.47 and 0.56 for APP mouse hippocampal regions. Furthermore, the storage modulus E' was obtained as a function of strain between 5 and 7.5% and showed a stiffening behavior with the strain $S = \Delta E'/\Delta\varepsilon$ in the range of 0.1–1.1 kPa/% for WT mouse and 0.2–1.6 kPa/% for APP. The stiffening with the strain S was higher for all APP/PS1 hippocampal subregions except SLM. Interestingly, stiffer regions were stiffening more than softer regions (see Fig. S.1). To summarize, APP/PS1 mouse hippocampus shows a higher degree of mechanical heterogeneity in terms of storage modulus and a higher degree of nonlinearity with the strain.

Although plaques were present in these slices as confirmed by fluorescent staining with Methoxy X-04, mechanical heterogeneity of each region was high for both WT and APP/PS1 (mean SD~40% and 37%, respectively) and the resolution was low (50–80 μm) when compared to the size of the plaques (~10–50 μm diameter Galea et al., 2015). Furthermore, the staining and imaging of plaques were done after the indentation measurements, making identification of plaques in mechanical maps less accurate due to shrinkage of the slice during fixation with PFA. Taken together, while differences in viscoelastic parameters between APP/PS1 and WT hippocampal regions were assessed, it was not possible to identify the mechanical properties of individual plaques with this indentation protocol.

3.2. High resolution plaque mapping

To directly measure the mechanical properties of the plaques, the same side of the slice needs to be indented and imaged, thereby, the bright-field inverted microscope was replaced with an upright fluorescence microscope (see Fig. 1D) and plaques were stained with Methoxy X-04 before starting the indentation measurements. The shallow-angle indentation probe was designed with a transparent cantilever to enable fluorescence imaging through the cantilever and a tip of R = 21 μm was

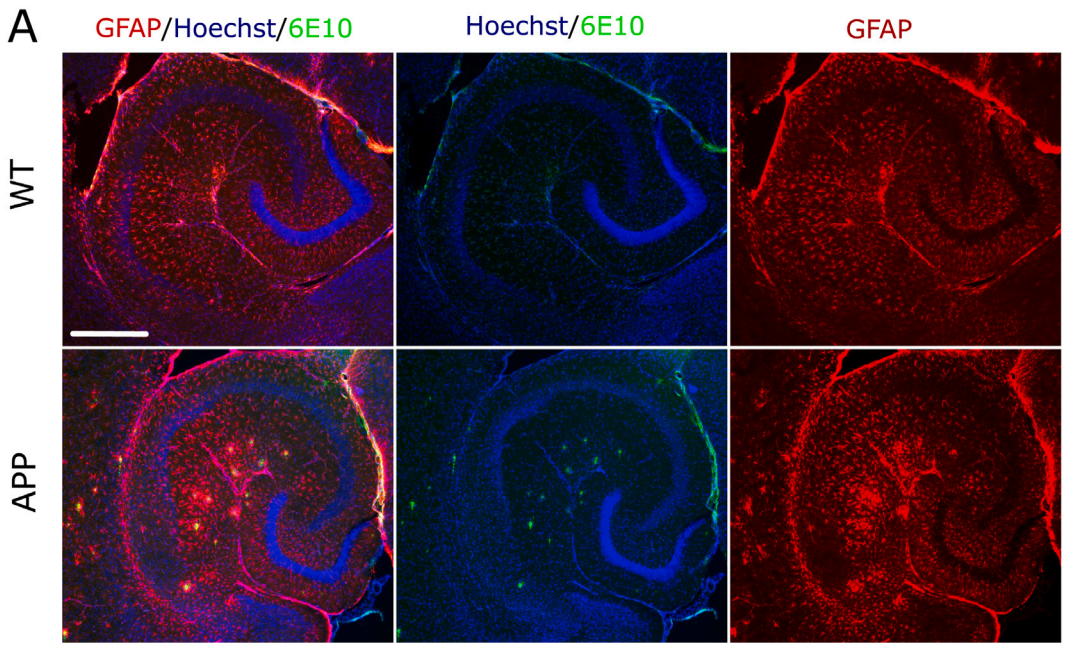

B

	ML	GCL	Hilus	CA3-SO	CA3-SP	CA3-SR	CA1-SR	SLM	Sub	Alv
mean	2.8	0	0.1	0	0	0.1	0.4	4.3	0.8	0.4
SD	2.6	0	0.3	0	0	0.3	0.7	2.3	1	0.6

Fig. 4. (A) Fluorescent images of 6-month-old WT and APP/PS1 mice hippocampus stained with GFAP (astrocytes), Hoechst(nuclei) and 6E10 (Aβ plaques). The scale bar (white line) is 500 μm. (B) Mean number of Aβ plaques per region in APP/PS1 mice hippocampal slices (number of animals n = 3, number of slices N = 15).

chosen to increase mapping resolution (5–9 μm). Fig. 3 shows Young's modulus maps of the plaques and the surrounding areas. In none of Young's modulus maps, the plaques show strikingly different mechanical properties from the surroundings, although regional mechanical heterogeneity was high with a standard deviation between 39 and 52%.

3.3. (Immuno)histochemical comparison

To investigate the underlying relationship between changes in mechanical properties and brain tissue composition in APP/PS1 mice, we performed (immuno)histochemical staining of the cytoskeleton of astrocytes (GFAP), cell nuclei (Hoechst), and Aβ plaques (6E10) (see Fig. 4 A). APP/PS1 mouse hippocampus have stained positive for the Aβ plaques with the mean number of plaques per region given in Fig. 4 B. SLM region had the highest averaged number of plaques - 4.3 ± 2.6, followed by ML - 2.8 ± 2.3 and Sub - 0.8 ± 1, and all the other regions had rarely any plaques (<0.5). Furthermore, the plaques were surrounded by GFAP expressing astrocytes indicating astrogliosis. Comparing the mechanical data obtained in the SLM and Sub regions (where no stiffening of APP/PS1 was observed) to those obtained in the ML region (where the stiffening was significant), we can conclude that, within the error of our measurements, there is no clear relationship between the number of plaques and the stiffening behavior observed in our experiments. Additional WFA staining for perineural nets (PNNs) of extracellular matrix (ECM) and MBP for myelin did not show any qualitative differences in composition between APP and WT hippocampus (see Fig. S.2).

4. Discussion

By using depth-controlled oscillatory indentation mapping, we were able to obtain viscoelastic properties of 10 hippocampal subregions of APP/PS1 mice. We compared our results with data from WT mice and found that the former is stiffer (i.e. higher storage modulus) and has better capability to dissipate mechanical energy (i.e. higher damping factor)(Fig. 2). We also showed that brain tissue from APP mice stiffens more with the strain and is more heterogeneous in terms of elasticity than WT mice (Fig. S.1). The number of plaques surrounded by upregulated GFAP astrocytes differs between the regions but does not correlate with changes in viscoelastic parameters. Nevertheless, the increased viscoelasticity, both elastic resistance and viscous dissipation, suggests that there are structural changes that take place during the development of plaques in the APP/PS1 mouse model that could affect the physiology of the brain. For example, one could speculate that similarly to how stiff brain implants induces an inflammatory response (Moshayedi et al., 2014), brain stiffness change could contribute to the inflammatory response in Alzheimer's disease. In addition, there has been a number of MRE studies showing changes of viscoelastic parameters in various neuroinflammatory disorders (Gerischer et al., 2018; Riek et al., 2012; Millward et al., 2015; Fehlner et al., 2016; Schregel et al., 2012; Wuerfel et al., 2010).

APP/PS1 mouse model does not fully recapitulate AD disease in humans. It shows pathological features associated with amyloid deposition and lacks tauopathies (Sasaguri et al., 2017; Balducci and Forloni, 2011). Regarding structural changes, it has been reported previously that APP/PS1 mouse brain has a decreased amount of myelin (Menal et al., 2018), an increased level of ECM proteins (Vé et al., 2014) and increased astrogliosis, marked by upregulation of GFAP expression surrounding plaques (Kamphuis et al., 2012). In this study, we performed (immuno)histochemical stainings (Fig. 4 and Fig. S.2) of cell nuclei (Hoechst), the cytoskeleton of astrocytes (GFAP), myelin (MBP), PNNs (WFA) and Aβ plaques (6E10) in an attempt to understand which structural components cause changes in viscoelastic parameters of APP/PS1 mouse hippocampus. We observed a higher expression of GFAP and the presence of Aβ plaques in APP/PS1 mice compared to WT. However, there were no qualitative differences in other stained components and correlation with viscoelastic parameters

was not found. To better understand the structure-stiffness relationship, a more detailed quantitative study of brain tissue composition and organization is needed. The connection between brain compositions and its viscoelasticity is probably not a simple linear but a complex one with multiple interdependent variables such as alignment of fibers, density, size and type of cells, architecture and composition of extracellular matrix or fraction of water and lipids in the tissue. Furthermore, future studies should include multiple age groups from early to later stages of the disease to determine the onset of mechanical alterations.

Previously, MRE and atomic force microscopy (AFM) techniques have been used to compare healthy and AD mouse brains. AFM study on the fixated brain hippocampus reported lower Young's modulus values for AD than healthy mice (40 and 104 kPa, respectively) although measurements were performed at the nm scale and the measured subfields were not mentioned (Zhao et al., 2019). Another AFM study has shown that Young's modulus of fresh AD mouse brain tissue was lower than that of WT (0.4 and 0.7 kPa, respectively) when measured at 1.5 μm indentation-depth, although measurements were performed on cortex (Menal et al., 2018). Unfortunately, the noise level of the indentation system used in this study was relatively high due to the perfusion flow, thus, it was not possible to fit the data below 1 μm indentation-depth. MRE studies on mice, similar to humans (described in the introduction), have demonstrated a decrease in stiffness of AD mouse model brains in comparison to WT (Murphy et al., 2012; Munder et al., 2018), although the amount of deformation in terms of shear wave amplitude is at the μm scale and axial resolution is at ~mm scale. Our results are obtained by inducing deformation at a tissue scale i.e. 4–15 μm indentation-depth and spatially resolving individual brain regions at ~50 μm axial resolution. Deforming tissue at different scales results in the sensing of different structures. For example, when using small tips of AFM (<10 μm), one measures individual cells, subcellular structures, or other individual brain tissue components while during microindentation and MRE, the whole tissue is deformed resulting in the mechanical response from multiple cells, fibers, vessels within ECM. On the other hand, MRE provides averaged response of the entire region, e.g., hippocampus rather than individual hippocampal layers, such as when measured by indentation. Furthermore, as the brain is an anisotropic material, it is plausible that its response to different deformation modes or directions might vary, such as between compression and shear or in the parallel and perpendicular direction to WM fiber tracts. Finally, MRE measurements are performed *in vivo* where the brain is intact and under intracranial pressure while indentation is performed on brain tissue slices. Therefore, all of these factors contribute to the discrepancy between AFM, microindentation, and MRE studies.

High-resolution indentation mapping was done by modifying the setup to the upright fluorescence imaging configuration to localize and directly indent on the plaques. To our knowledge, this is the first study attempting to measure Young's modulus of plaques within brain tissue slices by deformation. However, the mechanical heterogeneity of the regions was high (SD~40%) and the mechanical properties of individual plaques were not distinguishable from the surroundings (Fig. 3). A previous study by Brillouin scattering spectroscopy on fixated mouse brain tissue slices has shown that only the core of the plaque was ~20% more elastic than surrounding tissue with a thin softer lipid ring around it, which could explain why we were not able to capture Young's modulus of individual plaques at a lower resolution (Mattana et al., 2017). Furthermore, it is worth mentioning that several other studies have reported that individual amyloid fibrils are very stiff in comparison to other biological materials (Knowles and Buehler, 2011).

In this study, data from 6- and 9-month-old mice were merged because there was not enough indication that age is a significant factor (Section 2.4). Considering that the mice are already mature at 6 months of age and there are not any large changes in brain structure during adulthood (from 3 to 16 months (Wang et al., 2020)), it is plausible that mechanical differences between 6- and 9-month-old are negligible.

There are two main limitations of the experimental approach used in this study: (1) imaging with fluorescence microscopy does not indicate how deep the plaque is situated within the brain tissue thickness; (2) the surface of the brain slice is rough and damaged due to slicing procedure, which results in an error in estimating mechanical properties, especially at smaller indentation-depths. Therefore, future experiments should include three-dimensional imaging, such as confocal microscopy (Rosso et al., 2019; Staunton et al., 2016), to visualize how different structural components of the brain such as cells, ECM, neuronal projections, and plaques deform under compression and, thereby, extract their individual contribution to viscoelasticity.

Code availability

The computer code used to generate the results of this study is available on request from the corresponding author.

CRediT authorship contribution statement

Nelda Antonovaite: Conceptualization, Methodology, Software, Validation, Formal analysis, Investigation, Resources, Data curation, Visualization, Writing - original draft, Writing - review & editing. **Lianne A. Hulshof:** Investigation, Resources, Writing - review & editing. **Christiaan F.M. Huffels:** Resources, Writing - review & editing. **Elly M. Hol:** Conceptualization, Writing - review & editing. **Wytse J. Wadman:** Conceptualization, Supervision, Resources. **Davide Iannuzzi:** Conceptualization, Supervision, Funding acquisition, Writing - review & editing.

Declaration of competing interest

One or more of the authors of this paper have disclosed potential or pertinent conflicts of interest, which may include receipt of payment, either direct or indirect, institutional support, or association with an entity in the biomedical field which may be perceived to have potential conflict of interest with this work. For full disclosure statements refer to https://doi.org/10.1016/j.jmbbm.2021.104697. D.I. is co-founder and shareholder of Optics11.

N.A. is an employee at Optics11.

Data availability

All raw and processed data that support the findings of this study are available from the corresponding author upon request.

Acknowledgments

The research leading to these results has received funding from the European Research Council under the European Union's Seventh Framework Program (FP/2007–2013)/ERC grant agreement no. [615170] and the Alzheimer Society in the Netherlands (Alzheimer Nederland WE.03-2017-04). The authors further thank M. Marrese for fruitful discussions, E. Paardekam for manufacturing indentation probes, and T. Smit for providing brain tissue slices and support in the lab.

Appendix A. Supplementary data

Supplementary material related to this article can be found online at https://doi.org/10.1016/j.jmbbm.2021.104697.

References

Antonovaite, N., Beekmans, S.V., Hol, E.M., Wadman, W.J., Iannuzzi, D., 2018. Regional variations in stiffness in live mouse brain tissue determined by depth-controlled indentation mapping. Sci. Rep. 8.

Antonovaite, N., Hulshof, L.A., Hol, E.M., Wadman, W.J., Iannuzzi, D., 2020. Viscoelastic mapping of mouse brain tissue: Relation to structure and age. J. Mech. Behav. Biomed. Mater. 104159.

Balducci, C., Forloni, G., 2011. APP Transgenic mice: Their use and limitations. NeuroMol. Med. 13, 117–137.

Bigot, M., Chauveau, F., Beuf, O., Lambert, S.A., 2018. Magnetic resonance elastography of rodent brain. Front. Neurol. 9.

D'Amelio, M., Cavallucci, V., Middei, S., Marchetti, C., Pacioni, S., Ferri, A., Diamantini, A., De Zio, D., Carrara, P., Battistini, L., Moreno, S., Bacci, A., Ammassari-Teule, M., Marie, H., Cecconi, F., 2011. Caspase-3 triggers early synaptic dysfunction in a mouse model of alzheimer's disease. Nature Neurosci. 14, 69–76.

Eberle, D., Fodelianaki, G., Kurth, T., Jagielska, A., Mö, S., Ulbricht, E., Wagner, K., Taubenberger, A.V., Trä, N., Escolano, J.-C., Franklin, R., Vliet, K.J.V., Guck, J., 2018. Acute but not inherited demyelination in mouse models leads to brain tissue stiffness changes. BioRxiv 449603.

Fakhoury, M., 2018. Microglia and astrocytes in alzheimer's disease: Implications for therapy. Curr. Neuropharmacol. 16, 508–518.

Fehlner, A., Behrens, J.R., Streitberger, K.-J., Papazoglou, S., Braun, J., Bellmann-Strobl, J., Ruprecht, K., Paul, F., Wü, J., Sack, I., 2016. Higher-resolution MR elastography reveals early mechanical signatures of neuroinflammation in patients with clinically isolated syndrome. J. Magn. Reson. Imaging 44, 51–58, _eprint: https://onlinelibrary.wiley.com/doi/pdf/10.1002/jmri.25129.

Franze, K., 2013. The mechanical control of nervous system development. Development (Cambridge, England) 140, 3069–3077.

Franze, K., Guck, J., 2010. The biophysics of neuronal growth. Rep. Progr. Phys. 73, 094601.

Galea, E., Morrison, W., Hudry, E., Arbel-Ornath, M., Bacskai, B.J., Gómez-Isla, T., Stanley, H.E., Hyman, B.T., 2015. Topological analyses in APP/PS1 mice reveal that astrocytes do not migrate to amyloid-beta plaques. Proc. Natl. Acad. Sci. 112, 15556–15561, Publisher: National Academy of Sciences Section: Physical Sciences.

Garcia-Alloza, M., Robbins, E.M., Zhang-Nunes, S.X., Purcell, S.M., Betensky, R.A., Raju, S., Prada, C., Greenberg, S.M., Bacskai, B.J., Frosch, M.P., 2006. Characterization of amyloid deposition in the appswe/PS1de9 mouse model of alzheimer disease. Neurobiol. Dis. 24, 516–524.

Georges, P.C., Miller, W.J., Meaney, D.F., Sawyer, E.S., Janmey, P.A., 2006. Matrices with compliance comparable to that of brain tissue select neuronal over glial growth in mixed cortical cultures. Biophys. J. 90, 3012–3018.

Gerischer, L.M., Fehlner, A., Kö, T., Prehn, K., Antonenko, D., Grittner, U., Braun, J., Sack, I., Flö, A., viscoelasticity, Combining., 2018. Combining viscoelasticity diffusivity and volume of the hippocampus for the diagnosis of alzheimer's disease based on magnetic resonance imaging. NeuroImage: Clin. 18, 485–493.

Hall, C.M., Moeendarbary, E., Sheridan, G.K., 2020. Mechanobiology of the brain in ageing and alzheimer's disease. Eur. J. Neurosci..

Herbert, E.G., Oliver, W.C., Pharr, G.M., 2008. Nanoindentation and the dynamic characterization of viscoelastic solids. J. Phys. D: Appl. Phys. 41, 074021.

Hiscox, L.V., Johnson, C.L., Barnhill, E., McGarry, M.D.J., Huston 3rd, J., v. Beek, E.J.R., Starr, J.M., Roberts, N., 2016. Magnetic resonance elastography (MRE) of the human brain: technique, findings and clinical applications. Phys. Med. Biol. 61, R401.

Hiscox, L.V., Johnson, C.L., McGarry, M.D.J., Marshall, H., Ritchie, C.W., van Beek, E.J.R., Roberts, N., Starr, J.M., 2020. Mechanical property alterations across the cerebral cortex due to alzheimer's disease. Brain Commun. 2, Publisher: Oxford Academic.

Kamphuis, W., Mamber, C., Moeton, M., Kooijman, L., Sluijs, J.A., Jansen, A.H.P., Verveer, M., de Groot, L.R., Smith, V.D., Rangarajan, S., Rodríguez, J.J., Orre, M., Hol, E.M., 2012. GFAP Isoforms in adult mouse brain with a focus on neurogenic astrocytes and reactive astrogliosis in mouse models of alzheimer disease. PLoS One 7, e42823.

Kihan Park, n., Lonsberry, G.E., Gearing, M., Levey, A.I., Desai, J.P., 2019. Viscoelastic properties of human autopsy brain tissues as biomarkers for alzheimer's diseases. IEEE Trans. Bio-Med. Eng. 66, 1705–1713.

Knowles, T.P.J., Buehler, M.J., 2011. Nanomechanics of functional and pathological amyloid materials. Nat. Nanotech. 6, 469–479.

Koser, D.E., Thompson, A.J., Foster, S.K., Dwivedy, A., Pillai, E.K., Sheridan, G.K., Svoboda, H., Viana, M., da F. Costa, L., Guck, J., Holt, C.E., Franze, K., 2016. Mechanosensing is critical for axon growth in the developing brain. Nature Neurosci. 19, 1592–1598.

Lacour, S.P., Courtine, G., Guck, J., 2016. Materials and technologies for soft implantable neuroprostheses. Nat. Rev. Mater. 1 (10), 1–14, Publisher: Nature Publishing Group.

Levy Nogueira, M., Epelbaum, S., Steyaert, J.-M., Dubois, B., Schwartz, L., 2016. Mechanical stress models of alzheimer's disease pathology. Alzheimer's Dement.: J. Alzheimer's Assoc. 12, 324–333.

Lin, D.C., Shreiber, D.I., Dimitriadis, E.K., Horkay, F., 2009. Spherical indentation of soft matter beyond the hertzian regime: numerical and experimental validation of hyperelastic models. Biomech. Model. Mechanobiol. 8, 345–358.

Mahumane, G.D., Kumar, P., d. Toit, L.C., Choonara, Y.E., Pillay, V., 2018. 3D Scaffolds for brain tissue regeneration: architectural challenges. Biomater. Sci. 6, 2812–2837, Publisher: The Royal Society of Chemistry.

Mattana, S., Caponi, S., Tamagnini, F., Fioretto, D., Palombo, F., 2017. Viscoelasticity of amyloid plaques in transgenic mouse brain studied by brillouin microspectroscopy and correlative Raman analysis. J. Innov. Opt. Health Sci. 10, 1742001.

Menal, M.J., Jorba, I., Torres, M., Montserrat, J.M., Gozal, D., Colell, A., Piñol Ripoll, G., Navajas, D., Almendros, I., Farré, R., 2018. Alzheimer's disease mutant mice exhibit reduced brain tissue stiffness compared to wild-type mice in both normoxia and following intermittent hypoxia mimicking sleep apnea. Front. Neurol. 9, Publisher: Frontiers.

Millward, J.M., Guo, J., Berndt, D., Braun, J., Sack, I., Infante-Duarte, C., 2015. Tissue structure and inflammatory processes shape viscoelastic properties of the mouse brain. NMR Biomed. 28, 831–839.

Montarolo, F., Parolisi, R., Hoxha, E., Boda, E., Tempia, F., 2013. Early enriched environment exposure protects spatial memory and accelerates amyloid plaque formation in appswe/PS1l166p mice. PLoS One 8, e69381, Publisher: Public Library of Science.

Moshayedi, P., Ng, G., Kwok, J.C.F., Yeo, G.S.H., Bryant, C.E., Fawcett, J.W., Franze, K., Guck, J., 2014. The relationship between glial cell mechanosensitivity and foreign body reactions in the central nervous system. Biomaterials 35, 3919–3925.

Munder, T., Pfeffer, A., Schreyer, S., Guo, J., Braun, J., Sack, I., Steiner, B., Klein, C., 2018. MR Elastography detection of early viscoelastic response of the murine hippocampus to amyloid beta accumulation and neuronal cell loss due to alzheimer's disease. J. Magn. Reson. Imaging 47, 105–114.

Murphy, M.C., Curran, G.L., Glaser, K.J., Rossman, P.J., Huston, J., Poduslo, J.F., Jack, C.R., Felmlee, J.P., Ehman, R.L., 2012. Magnetic resonance elastography of the brain in a mouse model of alzheimer's disease: initial results. Magn. Reson. Imaging 30, 535–539.

Murphy, M.C., Huston, J., Jack, C.R., Glaser, K.J., Manduca, A., Felmlee, J.P., Ehman, R.L., 2011. Decreased brain stiffness in alzheimer's disease determined by magnetic resonance elastography. J. Magn. Reson. Imaging: JMRI 34, 494–498.

Murphy, M.C., Jones, D.T., Jack, C.R., Glaser, K.J., Senjem, M.L., Manduca, A., Felmlee, J.P., Carter, R.E., Ehman, R.L., Huston, J., 2016. Regional brain stiffness changes across the alzheimer's disease spectrum. NeuroImage: Clin. 10, 283–290.

Osborn, L.M., Kamphuis, W., Wadman, W.J., Hol, E.M., 2016. Astrogliosis: An integral player in the pathogenesis of alzheimer's disease. Prog. Neurobiol. 144, 121–141.

Riek, K., Millward, J.M., Hamann, I., Mueller, S., Pfueller, C.F., Paul, F., Braun, J., Infante-Duarte, C., Sack, I., 2012. Magnetic resonance elastography reveals altered brain viscoelasticity in experimental autoimmune encephalomyelitis. NeuroImage : Clin. 1, 81–90.

Rosso, G., Liashkovich, I., Shahin, V., 2019. In situ investigation of interrelationships between morphology and biomechanics of endothelial and glial cells and their nuclei. Adv. Sci. 6, 1801638.

Ruan, L., Kang, Z., Pei, G., Le, Y., 2009. Amyloid deposition and inflammation in appswe/PS1de9 mouse model of alzheimer's disease. Curr. Alzheimer Res. 6, 531–540.

Sasaguri, H., Nilsson, P., Hashimoto, S., Nagata, K., Saito, T., De Strooper, B., Hardy, J., Vassar, R., Winblad, B., Saido, T.C., 2017. APP Mouse models for alzheimer's disease preclinical studies. EMBO J. 36, 2473–2487.

Schregel, K., Wuerfel, E., Garteiser, P., Gemeinhardt, I., Prozorovski, T., Aktas, O., Merz, H., Petersen, D., Wuerfel, J., Sinkus, R., 2012. Demyelination reduces brain parenchymal stiffness quantified in vivo by magnetic resonance elastography. Proc. Natl. Acad. Sci. USA 109, 6650–6655.

Smit, T., Deshayes, N.A.C., Borchelt, D.R., Kamphuis, W., Middeldorp, J., Hol, E.M., 2021. Reactive astrocytes as treatment targets in alzheimer's disease-systematic review of studies using the appsweps1de9 mouse model. Glia.

Staunton, J.R., Doss, B.L., Lindsay, S., Ros, R., 2016. Correlating confocal microscopy and atomic force indentation reveals metastatic cancer cells stiffen during invasion into collagen i matrices. Sci. Rep. 6 (1), 19686, Publisher: Nature Publishing Group.

Streitberger, K.-J., Sack, I., Krefting, D., Pfü, C., Braun, J., Paul, F., Wuerfel, J., 2012. Brain viscoelasticity alteration in chronic-progressive multiple sclerosis. PLoS One 7.

van Tijn, P., Dennissen, F.J.A., Gentier, R.J.G., Hobo, B., Hermes, D., Steinbusch, H.W.M., Van Leeuwen, F.W., Fischer, D.F., 2012. Mutant ubiquitin decreases amyloid beta plaque formation in a transgenic mouse model of alzheimer's disease. Neurochem. Int. 61, 739–748.

Tomba, C, Migdal, C., Fuard, D, Villard, C, Nicolas, A., 2019. Glial cell mechanosensitivity is reversed by adhesion cues.

Trinchese, F., Liu, S., Battaglia, F., Walter, S., Mathews, P.M., Arancio, O., 2004. Progressive age-related development of alzheimer-like pathology in APP/PS1 mice. Ann. Neurol. 55, 801–814.

2009. Ueber die Berührung fester elastischer Körper. J. Reine Angew. Math. (Crelle's J.) 1882, 156–171.

Urbanski, M.M., Brendel, M.B., Melendez-Vasquez, C.V., 2019. Acute and chronic demyelinated CNS lesions exhibit opposite elastic properties. Sci. Rep. 9 (1), 999, Publisher: Nature Publishing Group.

Vé, M.J., Heldring, C.M., Kamphuis, W., Hijazi, S., Timmerman, A.J., Li, K.W., van Nierop, P., Mansvelder, H.D., Hol, E.M., Smit, A.B., van Kesteren, R.E., 2014. Reducing hippocampal extracellular matrix reverses early memory deficits in a mouse model of alzheimer's disease. Acta Neuropathol. Commun. 2, 76.

Wang, S., Lai, X., Deng, Y., Song, Y., 2020. Correlation between mouse age and human age in anti-tumor research: Significance and method establishment. Life Sci. 242, 117242.

Wuerfel, J., Paul, F., Beierbach, B., Hamhaber, U., Klatt, D., Papazoglou, S., Zipp, F., Martus, P., Braun, J., Sack, I., 2010. MR-Elastography reveals degradation of tissue integrity in multiple sclerosis. NeuroImage 49, 2520–2525.

Yan, P., Bero, A.W., Cirrito, J.R., Xiao, Q., Hu, X., Wang, Y., Gonzales, E., Holtzman, D.M., Lee, J.-M., 2009. Characterizing the appearance and growth of amyloid plaques in APP/PS1 mice. J. Neurosci. 29, 10706–10714, Publisher: Society for Neuroscience Section: Articles.

Zhao, W., Cui, W., Xu, S., Cheong, L.-Z., Shen, C., 2019. Examination of alzheimer's disease by a combination of electrostatic force and mechanical measurement. J. Microsc. 275, 66–72.